

Light charged particle emission from hot $^{32}\text{S}^*$ formed in $^{20}\text{Ne} + ^{12}\text{C}$ reaction

Aparajita Dey^{*†}, S. Bhattacharya, C. Bhattacharya, K. Banerjee, T. K. Rana,

S. Kundu, S. R. Banerjee, S. Mukhopadhyay, D. Gupta[‡], R. Saha

Variable Energy Cyclotron Centre, Sector - 1, Block - AF, Bidhan Nagar, Kolkata - 700 064, India.

Inclusive energy distributions for light charged particles (p , d , t and α) have been measured in the ^{20}Ne (158, 170, 180, 200 MeV) + ^{12}C reactions in the angular range $10^\circ - 50^\circ$. Exclusive light charged particle energy distribution measurements were also done for the same system at 158 MeV bombarding energy by in-plane light charged particle – fragment coincidence. Pre-equilibrium components have been separated out from proton energy spectra using moving source model considering two sources. The data have been compared with the predictions of the statistical model code CASCADE. It has been observed that significant deformation effects were needed to be introduced in the compound nucleus in order to explain the shape of the evaporated d , t energy spectra. For protons, evaporated energy spectra were rather insensitive to nuclear deformation, though angular distributions could not be explained without deformation. Decay sequence of the hot ^{32}S nucleus has been investigated through exclusive light charged particle measurements using the ^{20}Ne (158 MeV) + ^{12}C reaction. Information on the sequential decay chain has been extracted through comparison of the experimental data with the predictions of the statistical model. It is observed from the present analysis that exclusive light charged particle data may be used as a powerful tool to probe the decay sequence of hot light compound systems.

PACS numbers: 24.60.Dr, 25.70.Pq, 25.70.Jj, 25.70.Gh

I. INTRODUCTION

Light charged particles (LCP) evaporated from an excited composite is widely used as a tool to investigate the properties of that composite. These emissions reflect the behavior of the composite at various stages of the deexcitation cascade. In light ion induced reaction the composite system gains low excitation and low angular momentum, while in heavy ion induced reaction the associated angular momentum value is high enough. The statistical model

* Electronic address: aparajita.dey@saha.ac.in

† Present Address: Saha Institute of Nuclear Physics, 1/AF, Bidhan Nagar, Kolkata - 700 064, India.

‡ Present Address: Bose Institute, Dept. of Physics and Centre for Astroparticle Physics and Space Science, Block EN, Sector V, Salt Lake City, Kolkata - 700 091, India.

is used to describe the decay of a highly excited composite. The energy spectra of light charged particles emitted in light ion induced reaction are explained satisfactorily by the statistical model predictions [1, 2]. However, in heavy ion induced reaction, the energy spectra of LCPs are inconsistent with the respective theoretical predictions of statistical model because of the angular momentum induced deformation of the hot composite [3]. In addition, specific structure effects (*i.e.*, α -clustering in α -like nuclei) are also known to influence the reaction process and thus contribute to the deformation of the composite.

The $^{20}\text{Ne} + ^{12}\text{C}$ system has been investigated extensively in recent years [4, 5, 6] in connection with the study of nuclear orbiting in α -cluster systems. As orbiting is associated with large deformation of the composite, the deformations of the hot composites formed in the $^{20}\text{Ne} + ^{12}\text{C}$ reactions (in the energy range 7 – 10 MeV/nucleon) have been estimated from the study of the respective α -evaporation spectra. It was found that the deformations of hot composites are much larger than “normal” deformation [5]. However, it is interesting to study if the emissions of other light particles are also equally affected by deformation. Here, we report a study on the effect of deformation in the emitted $Z = 1$ particles, such as, triton, deuteron, proton.

Very recently, there have been a few attempts [7, 8, 9, 10, 11] to measure the light charged particles in coincidence with individual evaporation residues to probe the finer details of the reaction mechanism. Such studies may enable us to explore the evaporation decay cascade of the composite system. Moreover, the contributions from other non-evaporative (*i.e.*, fissionlike, pre-equilibrium) decay channels may also be estimated from such measurement. Here, we report an exclusive measurement of light charged particles emitted in coincidence with individual evaporation residues of hot ^{32}S nucleus produced in the ^{20}Ne (158 MeV) + ^{12}C reaction and show that such exclusive data may provide important clues to reveal the intricacies of the decay cascade.

The paper has been arranged as follows. The experimental procedures are described in the Sec. II. The analysis of the data and the results are discussed in Sec. III. Finally, the summary and concluding remarks are given in Sec. IV.

II. EXPERIMENTAL DETAILS

The experiments were performed with accelerated ^{20}Ne ion beams of energies 158, 170, 180 and 200 MeV, respectively, from the Variable Energy Cyclotron at Kolkata. The target used was $\sim 550 \mu\text{g}/\text{cm}^2$ self-supporting ^{12}C . The intermediate mass fragments and evaporation residues have been detected using two solid state $\Delta E - E$ [$\sim 10 \mu\text{m}$ Si(SB) ΔE , $\sim 300 \mu\text{m}$ Si(SB) E] telescopes (THI) mounted on one arm of the 91.5 cm scattering chamber. The light charged particles have been detected using two solid state thick detector telescopes [$\sim 40, 100 \mu\text{m}$ Si(SB) ΔE , $\sim 5 \text{mm}$

Si(Li) E] (TLI) mounted on the other arm of the scattering chamber. Typical solid angles subtended by the telescopes were 0.33 msr, 0.19 msr, 0.74 msr and 0.53 msr, respectively. The telescopes were calibrated using elastically scattered ^{20}Ne ion from Au, Al and C targets and ^{228}Th α -source. Absolute energy calibrations of the E and ΔE detectors for each telescopes were done separately using standard kinematics and energy-loss calculations. The measured energies have been corrected for the energy losses at the target by incorporating a single average thickness correction for each fragment energy. The low-energy cutoffs thus obtained were typically ~ 3.0 MeV for proton and ~ 10.2 MeV for α -particles in TLI telescopes. In THI telescopes, the cutoffs were ~ 12.3 MeV for Boron and ~ 19.5 MeV for Oxygen. Well separated bands corresponding to elements having atomic numbers up to $Z = 13$ have been identified.

Inclusive energy distributions for light charged particles ($Z = 1, 2$) emitted in $^{20}\text{Ne} + ^{12}\text{C}$ reaction have been measured in the angular range 10° to 50° , in steps of 2.5° , at all bombarding energies. LCP energy spectra for $^{20}\text{Ne} + ^{27}\text{Al}$ at 158 MeV have also been measured for comparison. We have also measured the in-plane coincidence of light charged particles with intermediate mass fragments and evaporation residues (ER) for $^{20}\text{Ne} + ^{12}\text{C}$ at 158 MeV for the comparison of inclusive and exclusive spectra and to study the decay sequence of hot composite. A part of the present data (inclusive α -particle emission) has already been analysed and published elsewhere [5].

III. RESULTS AND DISCUSSIONS

Inclusive energy spectra for $Z = 1$ particles have been analysed for $^{20}\text{Ne} + ^{12}\text{C}$ reactions at 158, 170, 180 and 200 MeV in the angular range $10^\circ - 50^\circ$ to study the effect of nuclear deformation. It had been found from our previous study [5] that, the contribution of pre-equilibrium process is significant for proton emission at forward angles only and it becomes negligible at $\theta_{lab} \gtrsim 30^\circ$. Therefore, pre-equilibrium component was extracted from the forward angle ($\theta_{lab} \leq 30^\circ$) proton data, whereas effect of nuclear deformation was studied using the energy spectra of $Z = 1$ particles at $\theta_{lab} \gtrsim 30^\circ$, where pre-equilibrium effect is insignificant.

A. Proton emission: Pre-equilibrium processes

It is evident from Ref. [5] that the inclusive forward angle proton energy distributions have enhanced high-energy ‘tail’ when compared with those at backward angles (Fig. 1 in Ref. [5]). The backward angle spectra is usually believed to have originated from evaporative decay of compound nucleus, and the high energy tails observed in forward direction are considered to be the signature of pre-equilibrium emission. The shapes of the inclusive proton spectra have been

compared with the respective exclusive spectra (measured in coincidence with ER, $Z = 10 - 13$, at $\theta_{lab} = 10^\circ$) at the angles $\theta_{lab} = 15^\circ, 20^\circ, 35^\circ$ and 40° in Fig. 1. It is found that the shapes of the inclusive (filled circle) and exclusive (open circle) proton spectra are different for lower angles ($15^\circ, 20^\circ$) while, they are matching well for higher angles ($35^\circ, 40^\circ$). This indicates the presence of pre-equilibrium contributions to the proton spectra at forward angles. Cross-sections were normalized at one point for comparison.

The velocity contour maps of the Galilean-invariant differential cross-sections, $(d^2\sigma/d\Omega dE)/pc$, as a function of the velocity of the emitted protons provide an overall picture of the reaction pattern [12, 13, 14]. The velocity diagrams of invariant cross-sections in the $(v_{\parallel}, v_{\perp})$ plane for protons emitted in $^{20}\text{Ne} + ^{12}\text{C}$, ^{27}Al reactions at different bombarding energies have been displayed in Fig. 2. The size of the point is in proportion to the invariant cross-section. The arrows (lower velocity) indicate the compound nucleus velocity, v_{CN} . The solid circles correspond to the most probable average velocities of evaporated protons. It has been observed that for all bombarding energies, the invariant cross-sections do not follow the solid circle. This further indicates that some component which has higher velocity than v_{CN} is contributing to the proton emission spectra.

1. Extraction of pre-equilibrium component

From the above discussion it has been found that the slopes of the center-of-mass (c.m.) energy distributions (Fig. 1) of emitted protons depend on the emission angles and the invariant cross-section plotted in $(v_{\parallel}, v_{\perp})$ plane does not follow the circle centered around v_{CN} , the compound nucleus velocity. These observations indicate that the protons are not emitted entirely from a compound nuclear source; emission from other sources, moving with velocity higher than v_{CN} , should also be considered to explain the data.

To understand the nature of the sources, the proton energy spectra have been fitted using a phenomenological moving source model [13, 14, 15, 16, 17, 18] where it is assumed that the protons are emitted isotropically in the rest frame of moving sources. As there is evidence of pre-equilibrium component in proton spectra, it has been assumed that protons are emitted from two different sources: (i) equilibrium source having velocity v_0 and (ii) intermediate velocity source having velocity $v_1 > v_0$. Now the parametrization expression for double-differential cross section in laboratory rest frame is

$$\begin{aligned} \frac{d^2\sigma}{dE_{lab}d\Omega} = & C_1[(E_{lab} - V_{x1})E_{sx1}]^{3/2}exp(-E_{sx1}/T_1) \\ & + C_2[(E_{lab} - V_{x2})E_{sx2}]^{3/2}exp(-E_{sx2}/T_2), \end{aligned} \quad (1)$$

where

$$E_{sx1} = E_{lab} - V_{x1} + E_0 - 2[E_0(E_{lab} - V_{x1})]^{1/2} \cos\theta_{lab},$$

$$E_{sx2} = E_{lab} - V_{x2} + E_1 - 2[E_1(E_{lab} - V_{x2})]^{1/2} \cos\theta_{lab}.$$

where C_1 and C_2 are normalization constants, $E_1 = m_p v_1^2/2$ and V_{x1} , V_{x2} are Coulomb correction for the equilibrium source v_0 and intermediate velocity source v_1 , respectively. T_1 and T_2 are the temperatures of the two sources. In the first step, the energy spectrum at most backward angle (*i.e.*, at 50° in the present work) has been fitted using a single source. Then keeping these parameters fixed, the parameters of the faster moving source (v_1) have been extracted by two-source fitting. The optimized values for v_o , v_1 and T_1 , T_2 are given in Table I. The above procedure is illustrated in Fig. 3 by dashed line (C_1, v_0, T_1), dash-dot-dotted line (C_2, v_1, T_2) and solid line (total). It has been observed that v_o for protons are nearly equal to v_{CN} . The higher velocity arrows in Fig. 2 correspond to v_1 and dotted circles represent the average velocities of this type of source.

The center-of-mass angular distributions of the inclusive protons emitted in $^{20}\text{Ne} + ^{12}\text{C}$ reactions have been displayed as a function of the center-of-mass emission angles in Fig. 4. The equilibrium (circles) and pre-equilibrium (triangles) components of angular distribution have been shown. It is observed from the figure that for all bombarding energies, the differential cross-section for equilibrium component is proportional to $\exp(-\beta \sin^2 \Theta_{c.m.})$, which is the characteristic of the emission from a thermally equilibrated system [12]. For a thermally equilibrated system the c.m. angular distributions are fitted with the following expression:

$$(d\sigma/d\Omega)_{c.m.} = a \exp(-\beta \sin^2 \Theta_{c.m.}) \quad (2)$$

where, a is a normalization constant

and

$$\beta = \frac{\hbar^2(j+1/2)^2}{2IT} \frac{\mu R^2}{\mathcal{I} + \mu R^2}, \quad (3)$$

\mathcal{I} is moment of inertia, T is temperature, j is angular momentum and μR^2 is the moment of inertia of reduced system. In Fig. 4 the solid lines represent the fits with Eq. 2. The fitted value of the anisotropy parameter, β_{fitted} , is given in Table II. The angular distributions for pre-equilibrium component fall off faster than that for equilibrium component as function of angles in case of all bombarding energies. The c.m. angular distributions for proton emitted in ^{20}Ne (158 MeV) + ^{27}Al reaction has also been shown in Fig. 4.

B. Statistical model analysis using CASCADE

The analysis has been performed using the standard statistical model code CASCADE [19]. In the statistical model calculations, the lower energy part of the LCP spectrum is controlled by the transmission coefficients. The high energy part of the spectrum is controlled by the level density (E^*, j) and for a given angular momentum j and excitation energy E^* , it is defined as [1, 19]

$$\rho(E, j) = \frac{(2j+1)}{12} a^{1/2} \left(\frac{\hbar^2}{2\mathcal{I}_{eff}} \right)^{3/2} \times \frac{1}{(E+T-\Delta-E_j)^2} \exp \left[2[a(E-\Delta-E_j)]^{1/2} \right], \quad (4)$$

where a is level density parameter, T is the thermodynamic temperature, Δ is the pairing correction and E_j is the rotational energy written as

$$E_j = \frac{\hbar^2}{2\mathcal{I}_{eff}} j(j+1). \quad (5)$$

In hot rotating nuclei, the effective moment of inertia is taken to be spin dependent and is written as

$$\mathcal{I}_{eff} = \mathcal{I}_o \times (1 + \delta_1 j^2 + \delta_2 j^4), \quad (6)$$

where, the rigid-body moment of inertia, \mathcal{I}_o , is given by

$$\mathcal{I}_o = 2/5 A^{5/3} r_o^2. \quad (7)$$

Nonzero values of the deformability parameters δ_1 and δ_2 introduce the spin dependence in the effective moment of inertia [5, 20, 21].

The most sensitive parameters influencing the calculated light charged particle energy spectra are the critical angular momentum j_{cr} , the diffuseness parameter Δj , the level density parameter a , the nuclear radius parameter r_o , the transmission coefficients T_j , and the deformability parameters δ_1 and δ_2 .

The transmission coefficients are calculated using the optical model potential; The optical-model parameters for protons, deuterons and tritons were taken from Perey and Perey [22] whereas those for α -particles were taken from Huizenga and Igo [23]. The critical angular momentum for fusion, j_{cr} , was calculated using the Bass model [24] for each bombarding energy. The value of diffuseness parameter was taken as $2\hbar$ for all bombarding energies.

1. Level density parameter

The influence of the level density parameter, a , on the energy spectra is displayed in Fig. 5. The calculated spectra are shown for three values of a : (i) $A/8$ (solid line), (ii) $A/10$ (dashed line), and (iii) $A/12$ (dash-dotted line). The radius parameter r_o was taken to be 1.29 fm, following Pühlhofer *et al.* [19]. The angular momentum dependent deformability parameters (δ_1 and δ_2) were set equal to zero [1, 5, 20]. From Fig. 5, an increase in yield has been found in the high-energy tail of the light charged particle spectra as the value of the level density parameter is decreased. This is understood in a simple way: It can be seen from Eqn. 4 that the level density is exponentially proportional to the square root of a . This will reduce the level density when we reduce a and hence energetic particle emission will be favoured.

It has been found from Fig. 5 that the theoretical calculations fail to predict the overall shape of the experimental energy spectra of the light charged particles over the whole energy range except for protons. The value of $a = A/8$ reproduces the proton energy spectrum. Furthermore, the temperature (as well as excitation energy) dependence of a has been investigated recently [25, 26, 27, 28, 29]. The temperature dependence has been incorporated by introducing an inverse level density parameter $K(T)$. Then a becomes

$$a(T) = A/K(T) \quad (8)$$

where $K(T)$ is given by [30]

$$K(T) = \frac{15.5 \text{ MeV}}{1.6 + 1.8A^{-1/3} - 0.5\{1 - \exp[-(\frac{TA^{1/3}}{21 \text{ MeV}})^2]\}} \quad (9)$$

The K value calculated using this equation for $^{20}\text{Ne} + ^{12}\text{C}$ system is ~ 7.6 MeV in the excitation energy region 74 – 94 MeV ($E_{lab} = 145 - 200$ MeV). Therefore, a value of $a = A/8$ is reasonable.

2. Nuclear radius parameter and deformability parameters

The most sensitive input parameters are nuclear radius parameters and deformability parameters. Fig. 5 indicates that the slope of the LCP energy distributions are unexplained by the CASCADE predictions. It is well known fact that increasing the moment of inertia (according to the spin) decreases the slope of the yrast line at higher spin and hence increases the phase space available when emitting light charged particles with lower energies. The spin dependent moment of inertia is given by Eqn. 6. The slope of the spectra have been well reproduced by varying the parameters δ_1 and δ_2 . For different bombarding energies, different sets of δ_1 , δ_2 values were needed. The parameter δ_1

plays the main role in explaining the high-energy part of the data; it is also found to be quite sensitive to variation of the excitation energy of the system. However, a nonzero value of the parameter δ_2 is required to fit the high-energy-tail ($\gtrsim 20$ MeV) part of the data in particular, and it is found to be rather insensitive, to the variation of excitation energy, at least within the range of the present measurements. In addition, the radius parameter, r_o , was varied from 1.29 fm to 1.35 fm to take care of the low energy side of the experimental spectra. This change of r_o causes a shift of the peak of the energy distribution to low energy side and thus helps to fit the lower energy part of the data in a better way. The sensitivity of these nuclear radius parameter and deformability parameters were illustrated in Fig. 5 of Ref. [5] in details. The optimized values of the parameters are given in Table 1 of Ref. [5].

3. Energy distributions of $Z = 1$ particles

The inclusive energy spectra for triton have been shown in Fig. 6 at $E_{lab} = 158, 170, 180$ and 200 MeV for few representative laboratory angles. It has been found that the statistical model code CASCADE without deformation parameters ($r_o = 1.29$ fm, $\delta_1 = \delta_2 = 0$) [19] could not explain the experimentally measured spectra (dashed line). The CASCADE calculation using the deformation parameters ($r_o = 1.35$ fm, $\delta_1 \neq \delta_2 \neq 0$), which are estimated from α -particles spectra [5], explain the data very well (solid line).

The inclusive energy spectra for deuteron have been displayed in Fig. 7 at $E_{lab} = 158, 170, 180$ and 200 MeV for few representative laboratory angles. In this case also, the CASCADE calculations without deformation parameters do not reproduce the data (dashed line). The CASCADE calculations using the deformation parameters (Table 1 in Ref. [5]) estimated from α -particle spectra reproduce the data very well (solid line).

The inclusive proton energy spectra are shown in Fig. 8 for different bombarding energies (158, 170, 180 and 200 MeV). It is observed that proton spectra are not sensitive to the deformation of the composite. Dashed line shows the CASCADE calculation without deformation parameters. The calculation with deformation parameters are shown by solid lines. The high energy tail at forward angles is due to the pre-equilibrium processes which are unexplained by the CASCADE calculations. The exclusive proton spectra measured at $E_{lab} = 158$ MeV in coincidence with evaporation residues (at $\theta_{lab} = 10^\circ$) are shown in Fig. 9. The shape of these spectra are also insensitive to the deformation. The deformation parameters are $r_o = 1.35$ fm, $\delta_1 = 4.5 \times 10^{-3}$ and $\delta_2 = 2.0 \times 10^{-8}$ [5]. The protons emitted in the ^{20}Ne (158 MeV) + ^{27}Al reaction also show the similar characteristics (Fig. 10). For this system the deformation parameters are $r_o = 1.30$ fm, $\delta_1 = 4.5 \times 10^{-4}$ and $\delta_2 = 2.0 \times 10^{-8}$ and $r_{eff} = 1.51$ fm [5].

In order to investigate whether the deformation parameters thus obtained can consistently explain the angular

distribution data (Fig. 4), the values of the anisotropy parameter β obtained by fitting the angular distribution data using Eqn. 2, β_{fitted} , have been compared with those estimated from Eqn. 3 using the effective moment of inertia, \mathcal{I}_{eff} (Eqn. 6). Since \mathcal{I}_{eff} is angular momentum dependent, comparison was done for average angular momentum, j_{av} ($= \frac{2}{3}j_{cr}$). It is interesting to note here that the anisotropy parameters obtained directly by fitting the angular distribution data are in fair agreement with those estimated using the optimized deformation parameters obtained by statistical model fitting of the energy distribution data.

The β -values with no deformation (β_o , obtained using rigid body moment of inertia, \mathcal{I}_o) are found to be quite different from β_{fitted} ; so, angular distribution data cannot be explained properly (Fig. 11) with β_o . It is thus interesting to note that, though the proton energy distribution shapes are rather insensitive to the deformability parameters δ_1 , δ_2 , it is required to take the deformation into consideration to properly explain the angular distribution data.

C. Prediction of Decay sequence of hot ^{32}S nucleus

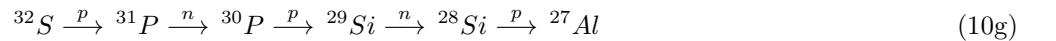
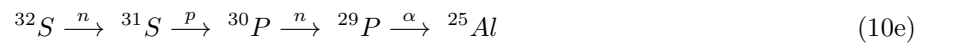
It is thus evident that the bulk (inclusive) emission data are found to be fairly well explained by ‘deformed’ statistical model predictions. However, it remains to be seen if emission at various stages may also be explained in a similar manner. Exclusive light charged particle emission data may be sensitive to this aspect as indicated earlier [7]. So, the decay sequence of the hot ^{32}S nucleus has been investigated through the exclusive light charged particle measurements using the ^{20}Ne (158 MeV) + ^{12}C reaction. Information on the sequential decay chain has been extracted through comparison of the experimental data with the predictions of the statistical model code CASCADE.

Inclusive energy distributions of heavy fragments (spectra having higher yields in Fig. 12) show that there are significant contribution from fusion-evaporation (FE) component. The arrows in Fig. 12 indicate the evaporation residue (ER) energy corresponding to the ER velocity $v_{CN} \cos \theta_{lab}$. The exclusive energy distributions of the heavy fragments (in coincidence with light charged particles) follow the statistical model prediction (PACE4 [31], solid curve in Fig. 12), which implies that the light charged particles measured in coincidence with Ne, Na, Mg and Al are emitted predominantly through FE channel, in the successive decay of hot ^{32}S compound nucleus. It is further noted that the heavy fragment spectra are skewed towards higher energy side, which are likely to be due to contributions from the residues of incompletely fused composites (in inverse kinematical systems, velocities of incomplete fusion residues are higher than those of complete fusion residues).

Some interesting features have been observed in the shapes of the α -particle spectra obtained in coincidence with

different evaporation residues (Fig. 13). The solid lines in Fig. 13 represent theoretical predictions of CASCADE [19] for the summed evaporation spectra of α -particles (sum of all α -particle spectra obtained in different decay cascade). A deformed configuration of compound nucleus, represented by the parameters $r_o = 1.35$ fm, $\delta_1 = 4.5 \times 10^{-3}$ and $\delta_2 = 2.0 \times 10^{-8}$ was used in this calculation. It has been shown in Ref. [5] that statistical model prediction using the above configuration was quite successful in explaining the α -particle spectra measured in coincidence with all evaporation residues ($Z = 10 - 13$, $\theta_{lab} = 10^\circ$) for the same reaction under consideration. However, the same prescription fails to explain the observed α -particle spectra (open circles) in coincidence with individual evaporation residues as evident from Fig. 13. It is indicative of the fact that the α -particles follow some specific decay path to populate a particular evaporation residue and the path is different as one goes from one residue to another. Thus, the study of light particle spectra in coincidence with individual residues is likely to reveal some interesting details of the compound nuclear decay sequence.

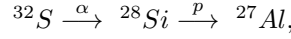
In order to understand the shapes of the exclusive α -particle energy spectra observed in coincidence with individual residue, α -particle evaporation spectra from each possible stage of the decay cascade populating a particular residue have been calculated and summed up with appropriate weightage to generate exclusive α -particle spectra corresponding to each residue; these spectra have then been compared with the respective experimental data. The procedure is illustrated as follows: Production of a typical evaporation residue, *e.g.*, Al, is possible through one of the following decay paths,



So, to generate the α -particle spectrum in coincidence with Al, the contribution of each decay path (10a – 10g) is added with the appropriate weightage factor (yield of decay path / total yield of all decay paths). This CASCADE prediction is shown by dashed line in Fig. 14. The similar procedure has been done for the proton spectra. It is interesting to find that the exclusive α -particle and proton spectra are still unexplained by the CASCADE predictions. The spectra

measured in-coincidence with Mg and Na are also unexplained by the spectra calculated using this technique (see Fig. 14).

The α -particles measured in coincidence with Al may be emitted from one or more of the following parent nuclei: ^{32}S , ^{31}S , ^{31}P , ^{30}P , ^{29}P . The experimentally measured α -particle spectra (open circle) in coincidence with Al have been displayed in Fig. 15. The theoretical α -particle spectra calculated from different stages of the decay cascade (*i.e.*, ^{32}S , ^{31}P , ^{31}S , ^{30}P , and ^{29}P) using CASCADE have also been displayed in Fig. 15 (represented by solid, dashed, dash-dotted, dotted and dash-dot-dotted lines, respectively). It is evident from Fig. 15 that the calculated first chance emission of α -particle from ^{32}S nucleus agrees well with the measured spectral shape. This is further supported by the proton spectra measured in coincidence with Al, which clearly indicate that the residue Al may be formed predominantly by the decay of ^{32}S nucleus through the emission of α -particle followed by a proton (path 10a), *i.e.*,



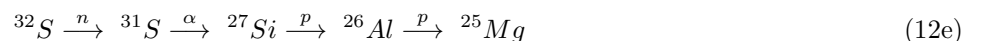
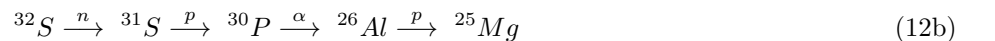
though relative α emission probabilities are comparable for both 10a and 10b paths.

The possible parent nuclei which may emit α -particles to populate Mg are ^{32}S , ^{31}P , ^{30}P , ^{30}Si and ^{28}Si . The measured α -particle spectra (open circles) in coincidence with Mg for different laboratory angles have been displayed in Fig. 16 along with the respective CASCADE predictions. The solid line corresponds to the total α -particle spectra obtained from the CASCADE calculation for the decay sequence:



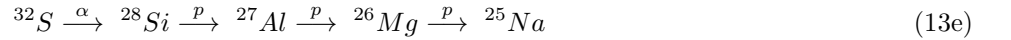
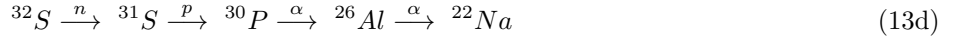
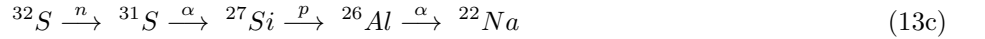
It is observed that this decay path reproduce the experimental spectra very well. The dash-dotted, dashed, dotted and dash-dot-dotted lines show the theoretical (CASCADE prediction) α -particle spectra for the nuclei ^{32}S , ^{31}P , ^{30}P and ^{30}Si , respectively.

The possible parent nuclei which may emit proton to populate Mg are ^{32}S , ^{31}S , ^{31}P , ^{28}Si , ^{27}Si , ^{27}Al and ^{26}Al . The possible decay sequences are



From Fig. 16, it is seen that the shapes of the experimental α -particle spectra are in fair agreement with the spectra obtained from decay path 12d (coincident with α -spectra from path 11), however, the experimental proton energy distributions match well with those of theoretical predictions for the case of proton emission from decay paths 12a and 12c. The α -particle spectra obtained from path 12c are very much different from the experimental spectra. The α -particle spectra from path 12a and the proton spectra from path 12d are in well agreement with lower energy part of the respective experimental spectra, though the higher energy parts remain unexplained. Therefore, from the analyses of exclusive proton and α -particle spectra measured in coincidence with Mg, it may be inferred that Mg may have been populated in the decay of ^{32}S nucleus through both $p - \alpha - p$ emission (decay path 12a) and $\alpha - p - p$ emission (decay path 12d), in addition to the exclusive 2α decay route (path 11). According to statistical model, the probability of different decay paths, through which Mg can be populated, decrease in the order 12a, 12c and 12d, and 11.

The α -particle and proton energy spectra measured in coincidence with the residue Na have been displayed in Fig. 17. The parent nuclei which may populate Na through α -particle emission are ^{32}S , ^{31}S , ^{31}P , ^{30}P , ^{27}Al and ^{26}Al . The protons may be emitted from ^{32}S , ^{31}S , ^{28}Si , ^{27}Si , ^{27}Al , ^{26}Mg nuclei. The different decay paths are



From Fig. 17 it is evident that the residue Na may have been populated predominantly through the sequence 13a (solid line). However, for the residue Na, 13a and 13b (dash-dotted line) decay paths have more or less equal probability. The other decay paths 13c (dotted line) and 13d (dashed line) have nearly same probabilities, which are five times smaller than the earlier two paths (13a and 13b).

Therefore, from this analysis it has been found that population of evaporation residue follows a specific decay path (solid lines in Fig. 14).

IV. SUMMARY

In this work, the $^{20}\text{Ne} + ^{12}\text{C}$ system has been studied at four incident energies, 158, 170, 180, and 200 MeV, respectively. The inclusive energy spectra of proton, deuteron and triton have been measured at different laboratory

angles in the range 10° to 50° . It was found that the invariant cross-section for protons plotted in $(v_{\parallel} - v_{\perp})$ plane does not follow the circle centered around compound nucleus velocity. This indicates the presence of a source which has velocity higher than v_{CN} . The effect of pre-equilibrium process has been found in the emitted proton spectra at forward angles ($\theta_{lab} \leq 30^\circ$). This pre-equilibrium component has been extracted using the moving source model considering two sources, equilibrium source and intermediate velocity source. The ^{20}Ne (158 MeV) + ^{27}Al reaction has been studied for comparison, and this also shows the presence of pre-equilibrium process.

It has been observed that nuclear deformation affected the energy distributions of different $Z = 1$ particles in different manner. The proton energy spectra were found to be rather insensitive to nuclear deformation for both the systems ($^{20}\text{Ne} + ^{12}\text{C}$, ^{27}Al) studied here. On the other hand, deuteron and triton energy spectra could not be explained without the introduction of deformation; in both cases (d and t), it was found that same set of spin dependent deformability parameters (δ_1, δ_2) which was required to fit the alpha-particle spectra [5], can explain the data fairly well. It is interesting to note here that for protons, though the the energy distributions are rather insensitive to nuclear deformation, proper explanation of the angular distributions of evaporated protons would require the deformation to be incorporated in the calculation, and the magnitudes of the deformation parameters were same as those used for fitting the d , t and α energy spectra. The sensitivity of the statistical model prediction of the energy spectra on level density parameter a has also been studied and it was found that the value of $a = A/8$ generated best fit to the data.

Some interesting features in the shapes of the exclusive light charged particle spectra have been observed in the decay of ^{32}S nucleus which may be correlated, at least in a qualitative manner, with the decay sequence of hot composite system. It may be inferred from the α -particle and proton spectra observed in-coincidence with Al that, the decay sequence in this case is first chance α emission followed by a proton emission. Similarly, in case of Mg, it may be inferred that Mg has been populated by sequential emission of α -particles from ^{32}S nucleus. In addition, Mg may also populate through $p - \alpha - p$ and $\alpha - p - p$ emission paths. For Na residue, $\alpha - p - \alpha$ is the most prominent decay path.

It is thus clear that, the exclusive fragment-light particle data may be used to extract information about the nuclear decay sequence. However, it is not intuitively evident why some particular decay paths would be favoured against other statistically competitive paths to populate a particular residue. More detailed exclusive measurements are required to have a concrete idea about the decay sequence. In addition, refinement of statistical model codes is also needed to tract down the complete decay sequence in more unambiguous manner.

Acknowledgments

The authors would like to thank the cyclotron operating staff for smooth running of the machine during the experiment and H. P. Sil for the fabrication of thin silicon detectors for the experiment.

-
- [1] J. R. Huizenga, A. N. Behkami, I. M. Govil, W. U. Schröder, and J. Töke, *Phys. Rev. C* **40**, 668 (1989).
 - [2] G. Viesti, B. Fornal, D. Fabris, K. Hagel, J. B. Natowitz, G. Nebbia, G. Prete, and F. Trotti, *Phys. Rev. C* **38**, 2640 (1988).
 - [3] T. C. Awes, G. Poggi, C. K. Gelbke, B. B. Back, B. G. Glagola, H. Breuer, V. E. Viola, Jr., *Phys. Rev. C* **24**, 89 (1981).
 - [4] C. Bhattacharya, *et al.*, *Phys. Rev. C* **72**, 021601R (2005).
 - [5] Aparajita Dey, S. Bhattacharya, C. Bhattacharya, K. Banerjee, T. K. Rana, S. Kundu, S. Mukhopadhyay, D. Gupta, and R. Saha, *Phys. Rev. C* **74**, 044605 (2006).
 - [6] Aparajita Dey, *et al.*, *Phys. Rev. C* **76**, 034608 (2007).
 - [7] D. Bandyopadhyay, C. Bhattacharya, K. Krishan, S. Bhattacharya, S. K. Basu, A. Chatterjee, S. Kailas, A. Shrivastava, and K. Mahata, *Phys. Rev. C* **64**, 064613 (2001).
 - [8] C. Bhattacharya, *et al.*, *Nucl. Phys.* **A654**, 841c (1999).
 - [9] J. Gomez del Campo, *et al.*, *Phys. Rev. C* **53**, 222 (1996).
 - [10] D. Shapira, *et al.*, *Phys. Rev. C* **55**, 2448 (1997).
 - [11] J. Gomez del Campo, *et al.*, *Phys. rev. C* **60**, 021601 (1999).
 - [12] W. E. Parker, *et al.*, *Phys. Rev. C* **44**, 774 (1991).
 - [13] Zhang Li, Wang Da-yan, Jin Gen-ming, Zhang Bao-guo, Wang Xi-ming, *Phys. Rev. C* **37**, 669 (1988).
 - [14] P. Belery, P. Cohilis, Th. Delbar, Y. El Marsi, Gh. Grégoire, *Phys. Rev. C* **36**, 1335 (1987).
 - [15] C. Bhattacharya, *et al.*, *Phys. Rev. C* **44**, 1049 (1991).
 - [16] C. Bhattacharya, S. Bhattacharya, and K. Krishan, *Z. Phys. A* **346**, 281 (1993).
 - [17] B. Borderie, *J. Phys. (Paris) Colloq.* **47**, C4-251 (1986), and references therein.
 - [18] C. Bhattacharya, *et al.*, *Phys. Rev. C* **52**, 798 (1995).
 - [19] F. Pühlhofer, *Nucl. Phys.* **A 280**, 267 (1977).
 - [20] D. Bandyopadhyay, C. Bhattacharya, K. Krishan, S. Bhattacharya, S. K. Basu, A. Chatterjee, S. Kailas, A. Srivastava, and K. Mahata, *Eur. Phys. J.* **A 14**, 53 (2002) and references therein.
 - [21] R. K. Choudhury, *et al.*, *Phys. Lett.* **143B**, 74 (1984).
 - [22] C. M. Perry, F. G. Perry, *At. Data Nucl. Data Tables* **17**, 1 (1976).

- [23] J. R. Huizenga and G. Igo, Nucl. Phys. **29**, 462 (1961).
- [24] R. Bass, Nuclear Reactions with Heavy Ions, (Springer-Verlag, Berlin, 1980) p. 256
- [25] D. Mahboub, *et al.*, Phys. Rev. C **69**, 034616 (2004).
- [26] G. Nebbia, *et al.*, Phys. Lett. **176B**, 20 (1986).
- [27] K. Hagel, *et al.*, Nucl. Phys. **A 486**, 429 (1988).
- [28] M. Gonin, *et al.*, Phys. Rev. C **42**, 2125 (1990).
- [29] A. Chbihi, L. G. Sobotka, N. G. Nicolis, D. G. Sarantites, D. W. Stracener, Z. Majka, D. C. Hensley, J. R. Beene, and M. L. Halbert, Phys. Rev. C **43**, 666 (1991).
- [30] J. P. Lestone, Phys. Rev. C **52**, 1118 (1995).
- [31] A. Gavron, Phys. Rev. C **21**, 230 (1980).

Tables

TABLE I: Optimized parameters from moving source model for protons.

E_{lab} (MeV)	v_{CN}/c	θ_{lab} (deg)	v_0/c	T_1 (MeV)	v_1/c	T_2 (MeV)
145	0.078	< 30	0.078(1)	2.0(1)	0.108(1)	2.5(2)
158	0.081	< 30	0.082(2)	2.1(1)	0.119(4)	2.7(1)
		> 30	0.082(2)	2.1(1)	-	-
170	0.084	< 30	0.085(1)	2.3(2)	0.122(2)	2.8(1)
		> 30	0.085(1)	2.3(1)	-	-
180	0.087	< 30	0.088(2)	2.4(1)	0.125(3)	2.9(2)
		> 30	0.088(2)	2.4(1)	-	-
200	0.091	< 30	0.093(2)	2.5(1)	0.131(3)	3.3(1)
		> 30	0.093(2)	2.5(1)	-	-

TABLE II: Anisotropy parameters for proton emitted at different energies.

Reaction	Energy (MeV)	β_{fitted}	β_{jav}	β_o
Ne + C	145	1.854 ± 0.504	1.641	5.678
	158	1.188 ± 0.323	1.279	5.408
	170	0.947 ± 0.163	1.041	4.937
	180	0.937 ± 0.108	0.939	5.116
	200	0.676 ± 0.164	0.844	4.911
Ne + Al	158	3.861 ± 0.183	3.663	5.964

Figures

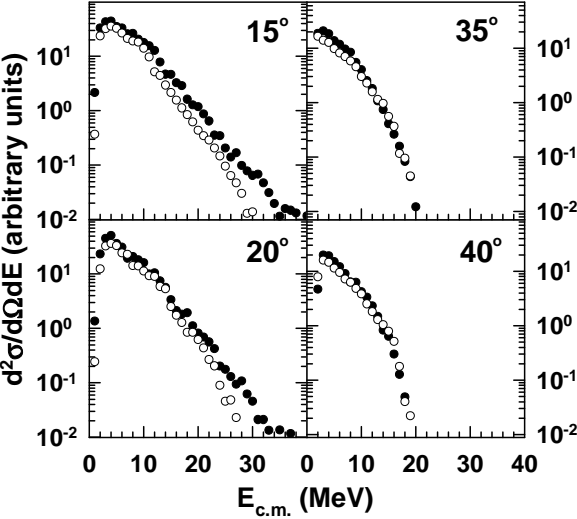


FIG. 1: Comparison between inclusive (\bullet) and exclusive (\circ) spectra for protons emitted in ^{20}Ne (158 MeV) + ^{12}C at different angles.

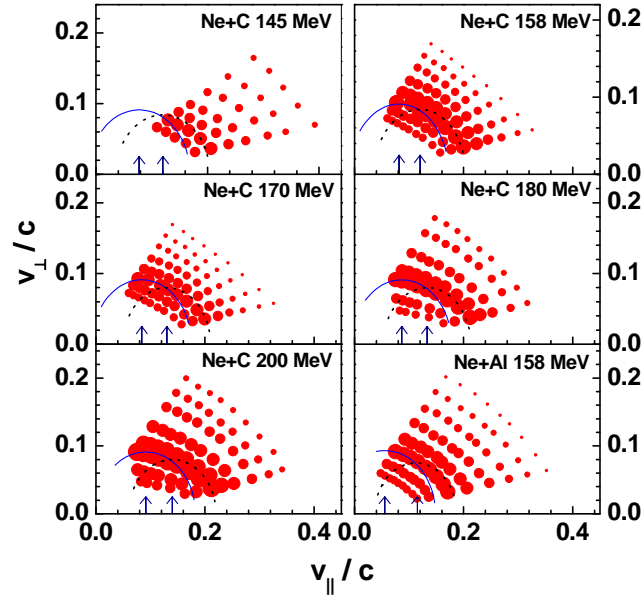


FIG. 2: (color online) The invariant cross section of protons plotted in $(v_{\parallel}, v_{\perp})$ plane at different energies. The arrows show the equilibrium source velocity (lower) and intermediate source velocity (higher). The most probable average velocities for equilibrium source (solid curve) and intermediate source (dotted curve) are shown for each energy (see text for details).

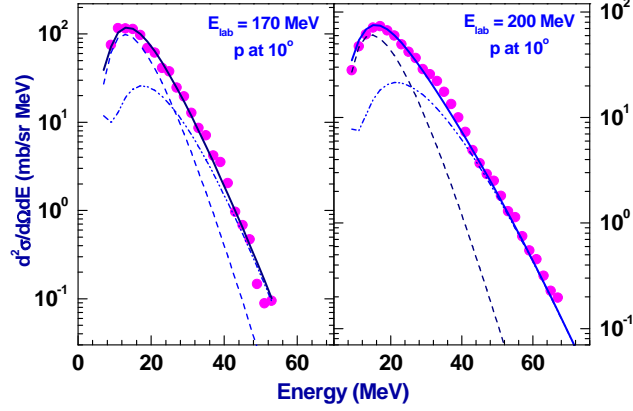


FIG. 3: (color online) The measured proton spectrum emitted in $^{20}\text{Ne} + ^{12}\text{C}$ reaction at $\theta_{lab} = 10^\circ$ for $E_{lab} = 170$ and 200 MeV. Experimental data is fitted with Eqn. 1. The dashed, dash-dot-dotted and solid lines correspond to the equilibrium source (v_o, T_1) , intermediate source (v_1, T_2) and total contribution, respectively.

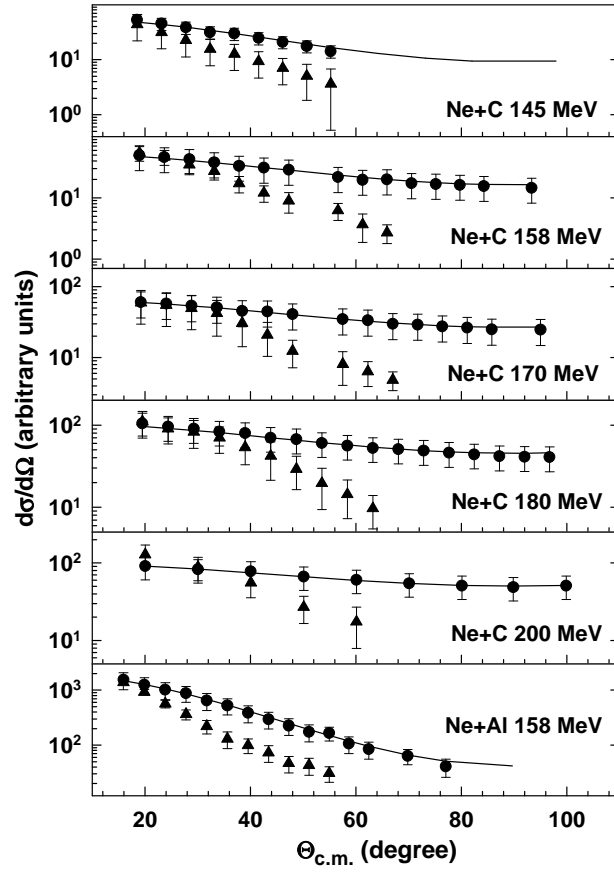


FIG. 4: The angular distributions for protons emitted in the $^{20}\text{Ne} + ^{12}\text{C}$, ^{27}Al reactions for different bombarding energies. The equilibrium (●) and pre-equilibrium (▲) components are shown. The solid curves are fit to the data using Eq. 2.

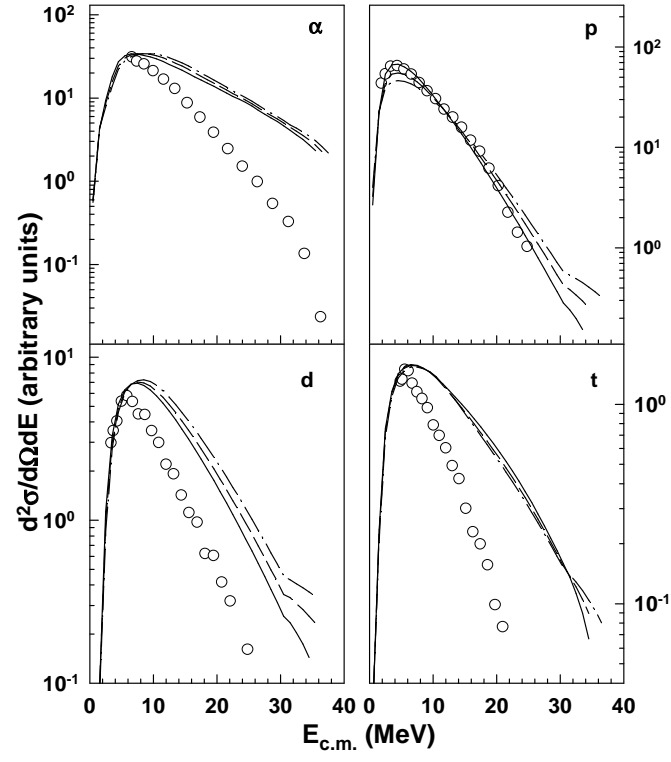


FIG. 5: Inclusive light charged particle (α , p , d , t) energy spectra at $\theta_{lab} = 40^\circ$ for ^{20}Ne (200 MeV) + ^{12}C reaction. The CASCADE predictions with $a = A/8$ (solid), $A/10$ (dashed), $A/12$ (dash-dotted) are shown.

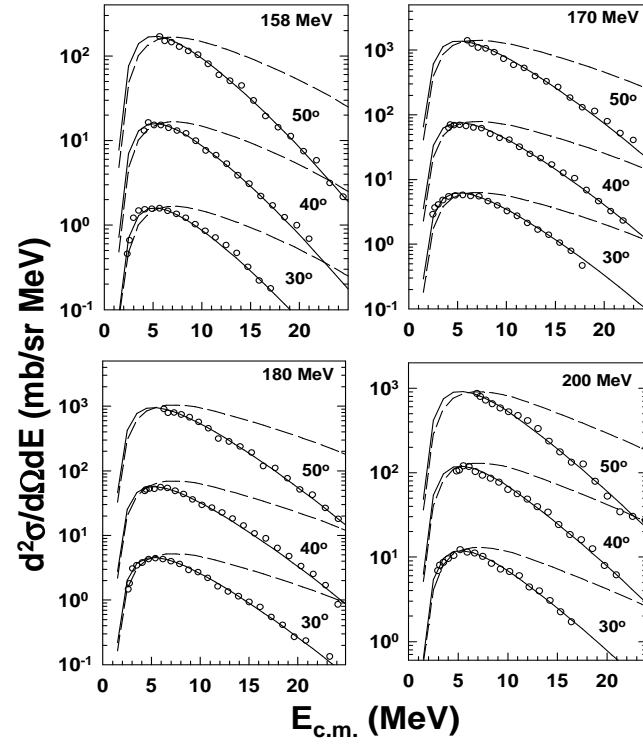


FIG. 6: Inclusive energy spectra for tritons emitted in ^{20}Ne (158, 170, 180, 200 MeV) + ^{12}C reactions at angles 30° ($\times 10^0$), 40° ($\times 10^1$) and 50° ($\times 10^2$). Dashed (solid) curves are the predictions of the statistical model code CASCADE without (with) deformation.

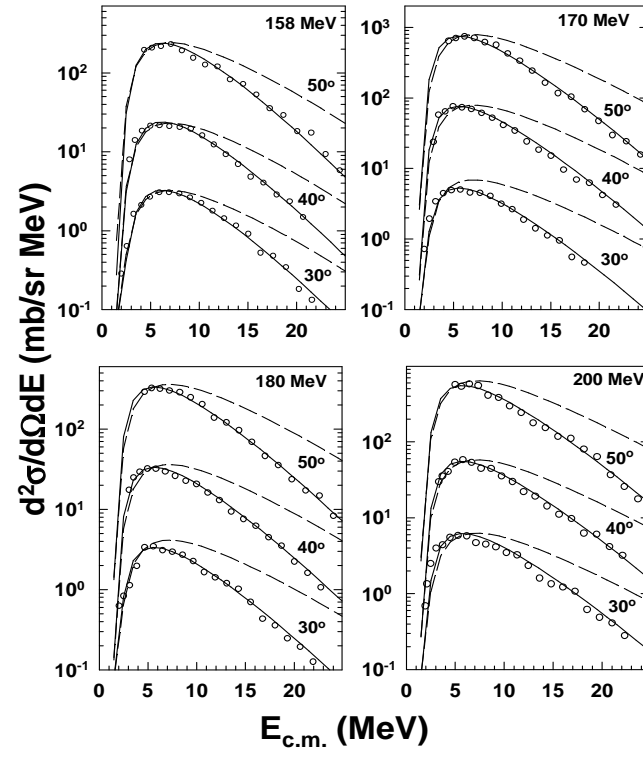


FIG. 7: Same as Fig. 6 for deuterons.

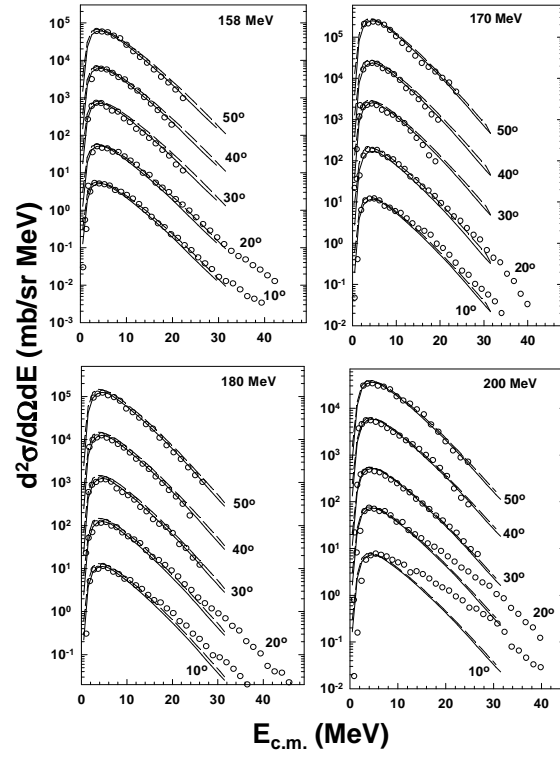


FIG. 8: Inclusive energy spectra for protons emitted in ^{20}Ne (158, 170, 180, 200 MeV) + ^{12}C reactions at the laboratory angles 10° ($\times 10^0$), 20° ($\times 10^1$), 30° ($\times 10^2$), 40° ($\times 10^3$) and 50° ($\times 10^4$). Dashed (solid) curves are the predictions of the statistical model code CASCADE without (with) deformation.

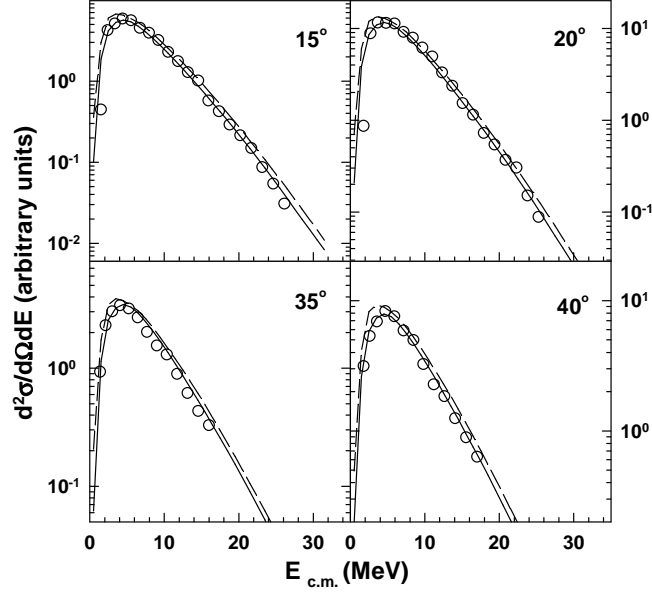


FIG. 9: Exclusive proton spectra at different θ_{lab} measured in coincidence with ERs ($10 \leq Z \leq 13$) emitted at $\theta_{lab} = 10^\circ$ in ^{20}Ne (158 MeV) + ^{12}C reaction. Dashed (solid) curves are the predictions of the statistical model code CASCADE without (with) deformation.

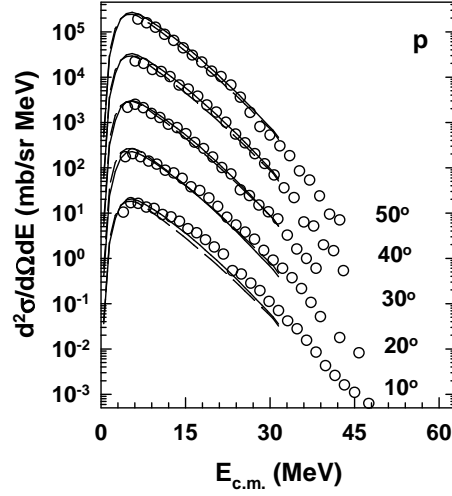


FIG. 10: Inclusive energy spectra for protons emitted in the ^{20}Ne (158 MeV) + ^{27}Al reaction at the laboratory angles 10° ($\times 10^0$), 20° ($\times 10^1$), 30° ($\times 10^2$), 40° ($\times 10^3$) and 50° ($\times 10^4$). Dashed (solid) curves are the predictions of the statistical model code CASCADE without (with) deformation.

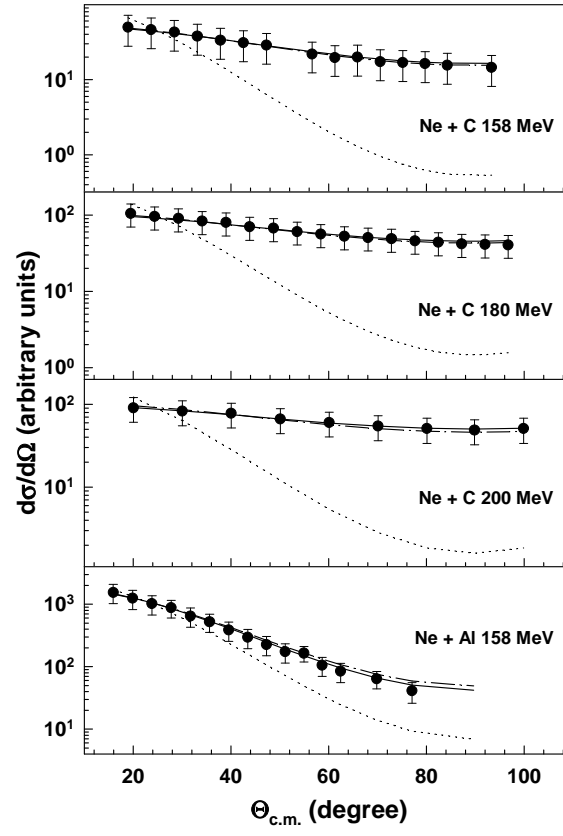


FIG. 11: The angular distributions for the equilibrium component of protons emitted in the $^{20}\text{Ne} + ^{12}\text{C}$, ^{27}Al reactions for different bombarding energies. The solid curves are fit to the data using Eq. 2. The dash-dotted and dotted curves correspond to the fit with β_{jav} and β_o , respectively.

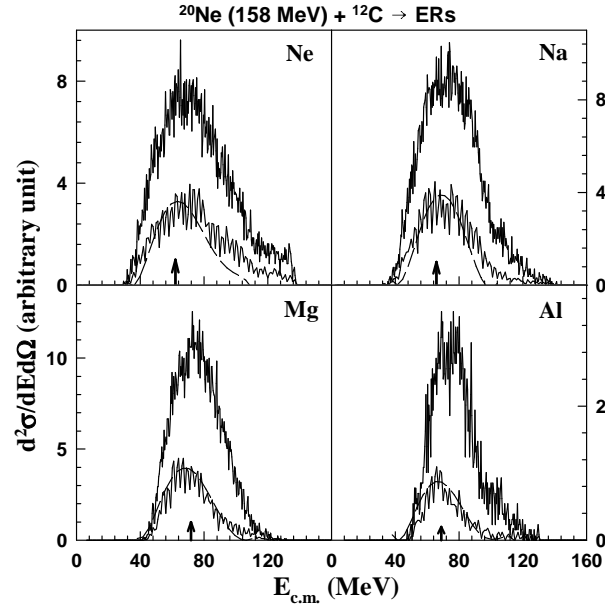


FIG. 12: Inclusive (higher yield) and exclusive (lower yield) energy spectra for Ne, Na, Mg and Al at $\theta_{lab} = 10^\circ$ along with the PACE4 prediction (dashed curve) [31]. The arrow shows the ER energy corresponding to $v_{CN} \cos \theta_{lab}$.

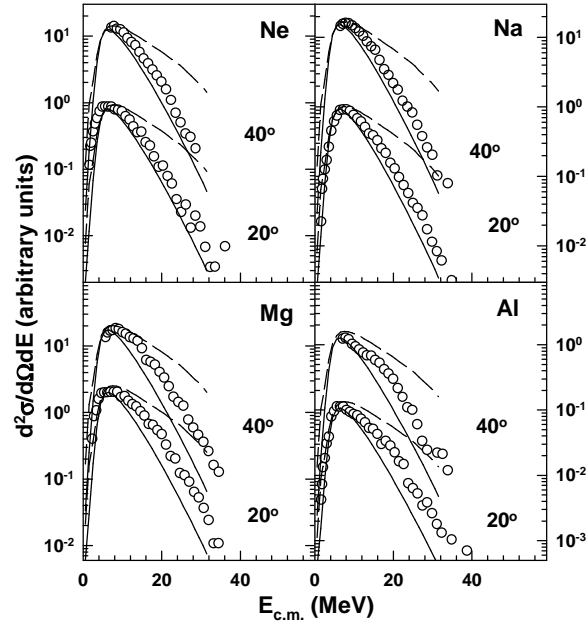


FIG. 13: Energy distributions of α -particles at $\theta_{lab} = 20^\circ$ and 40° measured in coincidence with Ne, Na, Mg and Al at $\theta_{lab} = 10^\circ$. Solid (dashed) lines are the predictions of code CASCADE with (without) deformation (see text).

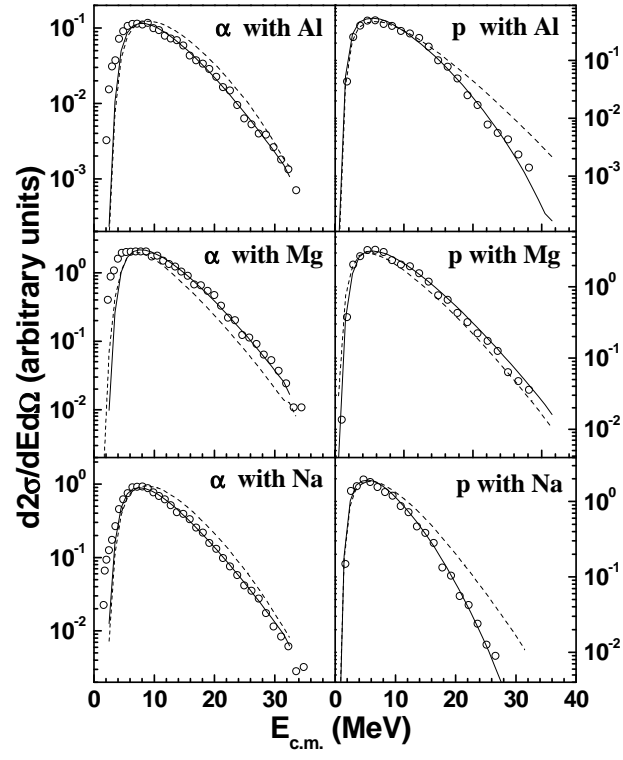


FIG. 14: α -particles and protons energy spectra measured at $\theta_{lab} = 20^\circ$ in coincidence with individual residue. Statistical model spectra are shown by dashed (sum of all possible decay path) and solid (particular decay path) curves (see text).

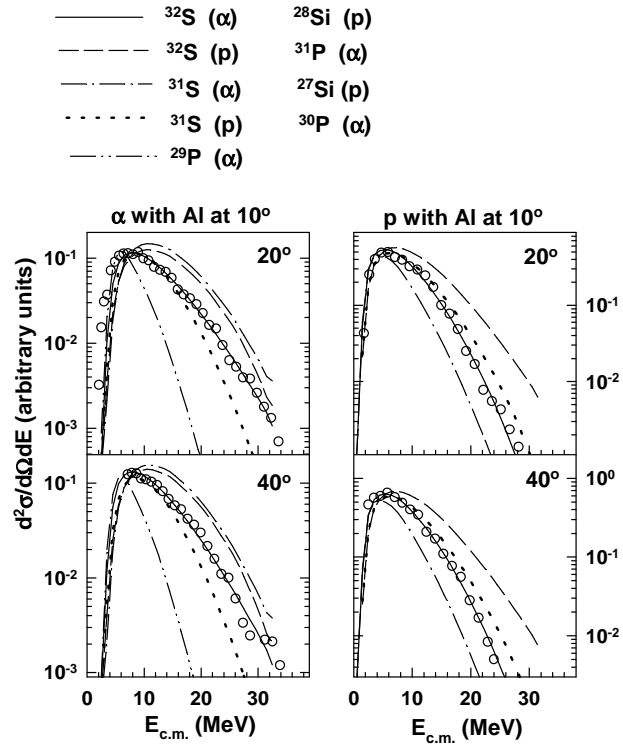
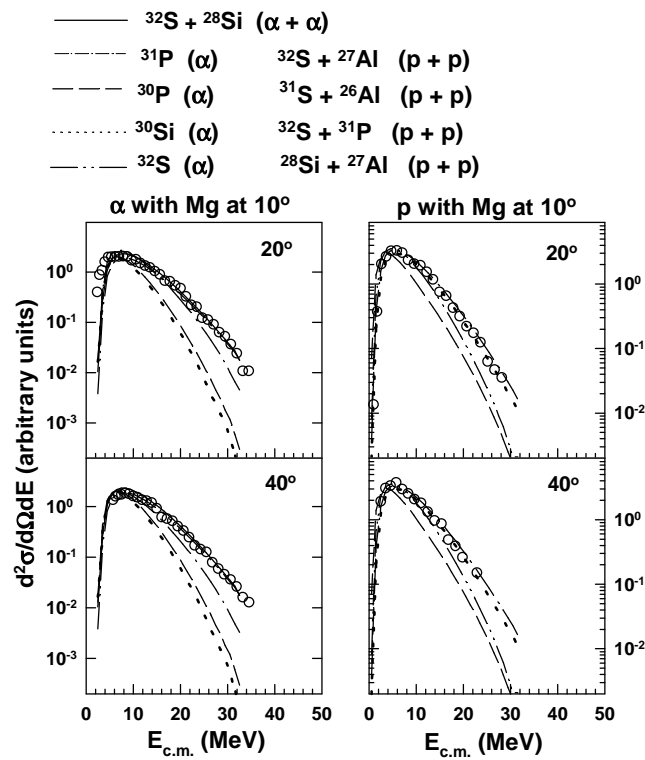
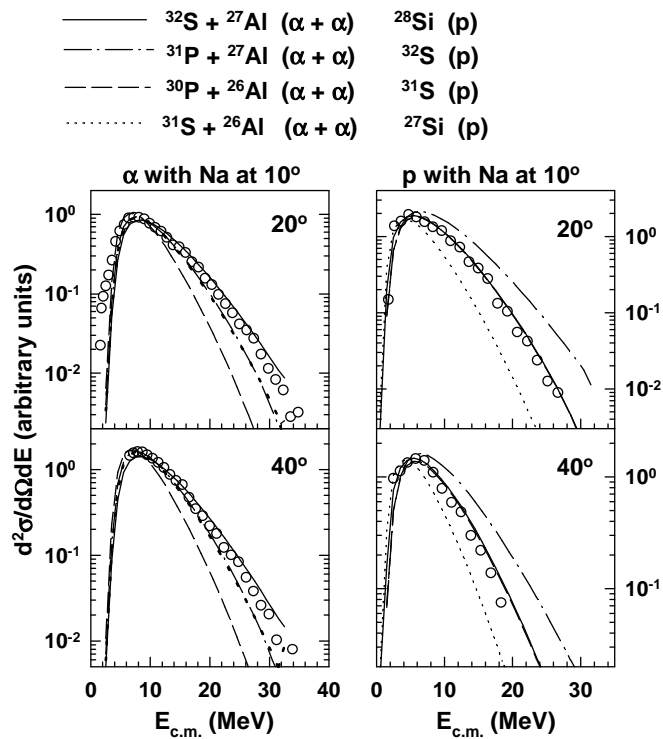


FIG. 15: Energy distributions of α -particles and protons measured in coincidence with Al at different laboratory angles. Different curves are the statistical model predictions using code CASCADE for the emission of α -particles and protons from different nuclei in the decay chain (see text).

FIG. 16: Same as Fig. 15 for α -particle and p in coincidence with Mg.FIG. 17: Same as Fig. 15 for α -particle and p in coincidence with Na.